A minor population of macrophage-tropic HIV-1 variants is identified in recrudescing viremia following analytic treatment interruption

Viviane M. Andrade[a], Carla Mavian[b], Dunja Babic[c], Thaissa Cordeiro[c], Mark Sharkey[c], Labelle Barrios[c], Christian Brander[d], Javier Martinez-Picado[d], Judith Dalmau[d], Anuska Llano[d], Jonathan Z. Li[e], Jeffrey Jacobson[f], Christy L. Lavine[g], Michael S. Seaman[g], Marco Salemi[b], and Mario Stevenson[c,h,1]

[a]Molecular Cell and Developmental Biology, Miller School of Medicine, University of Miami, Miami, FL 33136; [b]Emerging Pathogens Institute, University of Florida, Gainesville, FL 32610; [c]Department of Medicine, Miller School of Medicine, University of Miami, Miami, FL 33136; [d]Institut de Recerca de la Sida, 08916 Badalona, Spain; [e]Brigham and Women's Hospital, Harvard Medical School, Boston, MA 02115; [f]Lewis Katz School of Medicine, Temple University, Philadelphia, PA 19122; [g]Beth Israel Deaconess Medical Center, Harvard Medical School, Boston, MA 02215; and [h]Division of Infectious Diseases, Department of Medicine, University of Miami Miller School of Medicine, Miami, FL 33136

Edited by Stephen P. Goff, Columbia University Medical Center, New York, NY, and approved March 13, 2020 (received for review September 30, 2019)

HIV-1 persists in cellular reservoirs that can reignite viremia if antiretroviral therapy (ART) is interrupted. Therefore, insight into the nature of those reservoirs may be revealed from the composition of recrudescing viremia following treatment cessation. A minor population of macrophage-tropic (M-tropic) viruses was identified in a library of recombinant viruses constructed with individual envelope genes that were obtained from plasma of six individuals undergoing analytic treatment interruption (ATI). M-tropic viruses could also be enriched from post-ATI plasma using macrophage-specific (CD14) but not CD4+ T cell-specific (CD3) antibodies, suggesting that M-tropic viruses had a macrophage origin. Molecular clock analysis indicated that the establishment of M-tropic HIV-1 variants predated ATI. Collectively, these data suggest that macrophages are a viral reservoir in HIV-1–infected individuals on effective ART and that M-tropic variants can appear in rebounding viremia when treatment is interrupted. These findings have implications for the design of curative strategies for HIV-1.

macrophages | HIV-1 reservoirs | analytical treatment interruption

HIV-1 persists in infected individuals on suppressive antiretroviral therapy (ART) and efforts to develop a cure for HIV-1 infection include characterization of the reservoirs that sustain viral persistence. Most of the attention regarding the mechanism of viral persistence has focused on the reservoir of memory CD4+ T cells which harbor HIV-1 genomes in a latent state (1, 2). This research has been limited predominantly to analysis of peripheral CD4+ T cells. However, the contribution of tissue-resident cells, such as macrophages, to viral persistence remains unresolved. Macrophages are permissive to productive HIV-1 and Simian Immunodeficiency Virus (SIV) infection both in vitro (3) and in vivo (4). Infection of tissue macrophages in the Central Nervous System (CNS), lung, and lymph nodes of both viremic and aviremic nonhuman primates has been demonstrated (5–7). SIV nucleic acids can be detected in macrophages from infected macaques (8, 9). Rodent (10) and nonhuman primate models (7) have reconstituted latent infection of macrophages under ART. However, whether tissue macrophages in infected, aviremic individuals on ART harbor replication-competent HIV-1 and whether these macrophages constitute a functional reservoir capable of reigniting viremia when ART is interrupted remain unanswered.

Assessing the contribution of tissue resident macrophages to viral persistence is challenging. Macrophages are highly heterogenous and reside in tissues, such as the CNS, that are not accessible in living subjects. Examination of the composition of viremia that rebounds following analytic treatment interruption (ATI) can potentially provide insight into the nature of the reservoirs from which the rebounding viruses originated (11). This approach can avoid the limitations in tissue sampling and can provide an unbiased approach to assess the nature of the reservoirs in which biologically competent HIV-1 can persist in the face of suppressive ART.

We have adopted this approach to address the longstanding question of whether tissue macrophages support HIV-1 persistence in individuals on suppressive ART. We assessed whether any viruses populating post-ATI viremia exhibited macrophage tropism and contained markers indicative of a macrophage origin. We demonstrate the presence of a small number of highly macrophage-tropic (M-tropic) viruses in plasma of individuals undergoing ATI. We observed that some of these viruses display macrophage-specific markers that suggest they originated from macrophages. Furthermore, molecular clock analysis indicates that some of these variants were established prior to ART interruption. Collectively, our results suggest that tissue macrophages

Significance

Identifying cellular reservoirs contributing to HIV-1 persistence is essential for development of curative strategies for HIV-1. We identified M-tropic viruses in rebound viremia of individuals undergoing treatment interruption. In addition, some M-tropic viruses contained macrophage-specific markers on their surface, suggesting those M-tropic viruses had a macrophage origin. Molecular clock analysis further suggested that M-tropic variants predated treatment interruption in three of the subjects analyzed. Our results indicate that HIV-1–infected macrophages are present in individuals on effective ART and, as such, should be considered in the design of strategies aimed at eliminating the HIV-1 reservoir.

Author contributions: V.M.A., D.B., M. Sharkey, M.S.S., and M. Stevenson designed research; V.M.A., D.B., T.C., L.B., C.L.L., and M.S.S. performed research; C.M., C.B., J.M.-P., J.D., A.L., J.Z.L., J.J., M.S.S., and M. Salemi contributed new reagents/analytic tools; V.M.A., C.M., T.C., L.B., and M. Salemi analyzed data; and V.M.A., C.M., M. Salemi, and M. Stevenson wrote the paper.

The authors declare no competing interest.

This article is a PNAS Direct Submission.

Data deposition: All sequences reported in this paper have been deposited in the GenBank database, under the following accession numbers: 126G (MK250122–MK250216), PL102 (MK250217–250273), PL109 (MK250274–MK250362), PL216 (MK254784–MK254839), PL63 (MN395385 and MK250100–MK250121), and PL234 (MK254843, MK254890–MK254895, MK254897, MK254911, MK254912, MK254914–MK254952, MK254959–MK254964, and MK254967).

[1]To whom correspondence may be addressed. Email: MStevenson@med.miami.edu.

This article contains supporting information online at https://www.pnas.org/lookup/suppl/doi:10.1073/pnas.1917034117/-/DCSupplemental.

First published April 16, 2020.

serve as a viral reservoir in individuals on suppressive ART. These studies are important in the design of strategies through which to eliminate reservoirs of HIV-1 from infected individuals.

Results

To assess whether macrophages may support HIV-1 persistence under effective ART, we adopted an approach to survey posttreatment-interruption viremia for the presence of macrophage-adapted viruses. Expression of CD4 (the primary receptor for HIV-1) on macrophages is limiting (12), and, as a consequence, infection of a macrophage can be accomplished only by HIV-1 variants harboring an envelope glycoprotein with a high affinity for CD4 (13). A single plasma sample from six individuals who underwent ATI was collected during the period of viral recrudescence. As outlined in *SI Appendix*, Table S1, all subjects were on antiretroviral therapy for more than 2.5 y and had well-suppressed infections (*SI Appendix*, Table S1). cDNA was generated from plasma virion RNA, and individual viral envelopes were generated by single-genome amplification (SGA) and then used to construct recombinant, full-length infectious HIV-1 molecular clones (Fig. 1*A*).

Between 70 and 113 independent envelope clones were generated from each of six subjects (a total of 551 recombinant viruses were generated from the six subjects). Those clones were then assessed for biological activity by titration on TZM-Bl cells. All clones that were infectious for TZM-Bl cells (360 clones in total) were first assessed for fusogenicity in primary macrophages, which is the most proximal event to receptor binding. A modified fusion assay, originally developed to measure HIV-1 fusogenicity on CD4+ T cells (14), was used to assess the fusogenic capacities of the recombinant viruses on macrophages. In this assay, highly M-tropic laboratory controls (HIV-1 ADA, HIV-1 YU2) efficiently fused with primary macrophages as evidenced by the frequency of blue cells at 450 nm, while T cell tropic (T-tropic) laboratory controls (HIV-1 LAI, HIV-1 4013P) (13, 15) fused poorly with macrophages (Fig. 1*C*). This fusogenic phenotype of viral envelopes analyzed by this approach was preserved; no alteration in fusogenic capacity was observed with T-tropic controls inserted into the infectious molecular backbone (*SI Appendix*, Fig. S1). While the majority of recombinants harboring plasma-derived envelopes fused poorly with macrophages, a small number of clones (~3 to 4%) fused efficiently with macrophages, at levels observed for highly M-tropic laboratory controls (Fig. 1*D*). Representative fields are indicated for recombinant clones with high (>50% positive macrophages), intermediate (20 to 50% positive macrophages), and low (<20% positive macrophages) macrophage fusogenicity. The comparable fusogenicities of these patient-derived clones and M-tropic controls were further confirmed by flow cytometry (*SI Appendix*, Fig. S2).

Functional (infectious for TZM-bl cells) recombinant HIV-1 variants that exhibited high fusogenicity for macrophages (≥50% positive macrophages) were next assessed for replication capacity in macrophages, which is the most stringent determinant of macrophage tropism. A subset of recombinant clones harboring plasma-derived envelopes that were highly fusogenic for macrophages (denoted as "H" in Fig. 2*A*) also replicated in macrophages at >50% of those observed with highly M-tropic laboratory controls, such as HIV-1 ADA or HIV-1 YU2 (Fig. 2*A* and *SI Appendix*, Fig. S3). These clones were subsequently referred to as M-tropic. In contrast, clones with intermediate and low (designated "I" and "L") macrophage fusogenicities replicated poorly or did not replicate in macrophages (referred as T-tropic), a phenotype shared by the T-tropic laboratory controls LAI and 4013P. Therefore, only a subset of recombinants with a high degree of fusogenicity (fusing at >50% of macrophages) was able to replicate in macrophages (Fig. 2*A* and *SI Appendix*, Fig. S3). This is to be expected, since small differences in fusogenicity exhibited in the single-cycle fusion assay would be accentuated under conditions of a spreading infection.

It is possible that the ability of these recombinants to replicate in macrophages was simply a reflection of an increased entry fitness for any cell type. However, and in agreement with other studies (16), the M-tropic viruses had similar infectious capacity for CD4+ T cells to their T-tropic counterparts (*SI Appendix*, Fig. S4). Therefore, while M-tropic viruses had significantly higher entry fitness for macrophages compared to their T-tropic counterparts, they had comparable entry efficiencies to their T-tropic counterparts in CD4+ T cells (*SI Appendix*, Fig. S4). Of all 360 infectious molecular recombinants constructed from all subjects that were phenotyped, 12 (3 to 4%) were capable of replicating in macrophages and thus designated as M-tropic (Fig. 2*B*). No M-tropic envelopes were observed in PL109 and one clone from PL216 was found to have a borderline degree of macrophage tropism (Fig. 2*B* and *SI Appendix*, Fig. S3). The absence of highly M-tropic envelopes in these subjects may simply indicate that an insufficient number of envelopes were sampled. Thus, four of six subjects harbored viral envelopes that were highly macrophage tropic.

The neutralization sensitivity of paired M- and T-tropic viruses was next assessed for subjects PL234, PL63, PL102, and 126G in which M-tropic viruses were identified. As expected, M-tropic viruses were more sensitive to neutralization by soluble CD4 (sCD4) than their T-tropic counterparts, while no differences in neutralization sensitivity between M- and T-tropic viruses were observed for antibodies to a variety of envelope epitopes distal to the CD4-binding site (Fig. 2*C* and *SI Appendix*, Fig. S5). We conclude that post-ATI viremia contains virus variants with a high capacity for macrophage infection.

The presence of highly M-tropic viruses in post-ATI viremia infers the presence of infected macrophages, but does not prove a macrophage origin. Since nascent virions derive their membranes from the host cell membrane, they acquire proteins specific to that host cell. Therefore, if M-tropic viruses were indeed produced from macrophages, their membranes would be expected to contain macrophage-specific proteins (Fig. 3*A*). We examined antibodies to macrophage-specific proteins (CD163, CD14, CD71, and CD33) and selected CD14 (clone 61D3) as being able to selectively immunoprecipitate macrophage-derived virions—36-fold enrichment versus T cell-produced virus (Fig. 3*B*). Plasma was immunoprecipitated in parallel with CD14 and CD3 antibodies. Viral envelopes in the immunoprecipitates were then cloned by SGA and used to generate recombinant, infectious clones and tested for their ability to fuse with macrophages. CD14-enriched viruses from 126G and PL102 subjects contained envelopes with an enhanced ability to fuse with macrophages, whereas envelopes from CD3-enriched viruses were poorly fusogenic for macrophages (Fig. 3*C*). Next, antibody-enriched viruses, as well as M-tropic and T-tropic viruses derived from random screening (as detailed in Figs. 1 and 2), were assessed for replication capacity in macrophages. Recombinant viruses constructed with CD14-enriched envelopes from subjects 126G and PL102 replicated efficiently in macrophages and at levels comparable to those of M-tropic variants derived directly by random plasma screening and M-tropic laboratory controls (Fig. 3*D*). One CD14-derived envelope from PL63 was weakly M-tropic and replicated inefficiently in macrophages. None of the envelopes enriched with the CD3 antibody were capable of undergoing spreading infection in macrophages which is defined as envelopes with replication capacity ≥50% of that observed with M-tropic controls (YU2, ADA). M-tropic envelopes isolated from subject 126G by CD14 immunoprecipitation were closely related to M-tropic envelopes obtained by random screening of post-ATI plasma (Fig. 3*E* and *SI Appendix*, Fig. S7*C* and Table S5). In contrast, T-tropic envelopes obtained by CD3 immunoprecipitation were more closely related to T-tropic

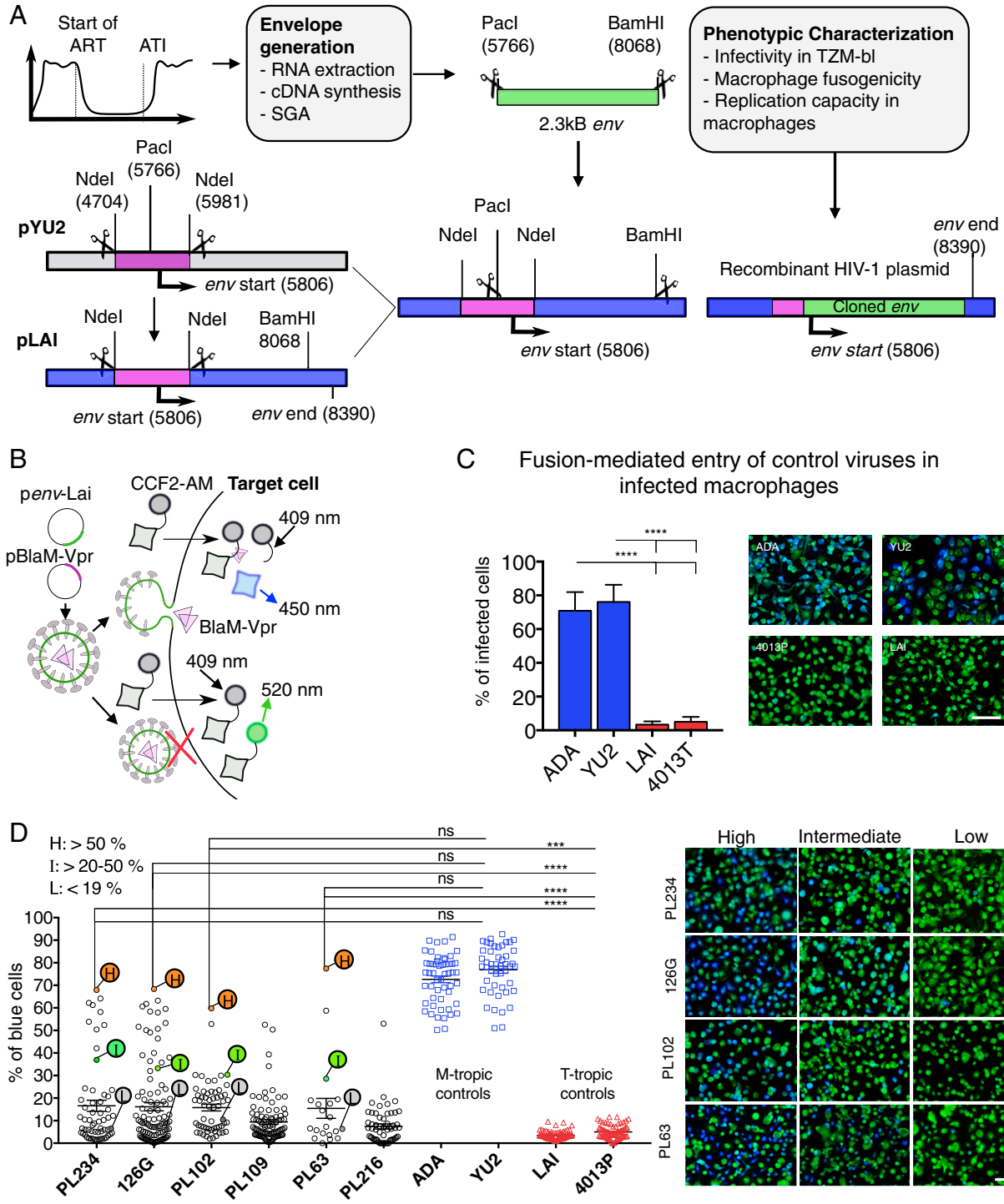

Fig. 1. Macrophage-adapted HIV-1 envelopes populate post-ATI viremia. (*A*) Schematic representation of the strategy for isolation of HIV-1 envelopes from plasma and construction of recombinant HIV-1 clones harboring envelopes from post-ATI viremia and laboratory controls (LAI, 4013P, ADA, and YU2). (*B*) Assessment of HIV-1 fusogenicity for primary macrophages. Data from ref. 14, which assesses hydrolyzation of CCF2 by an encapsidated β-lactamase. Hydrolyzed (indicative of fusion) and nonhydrolyzed CCF2-AM are distinguished by examination of infected cells at 450 nm. (*C*) Fusogenic capacities of macrophage and T-cell adapted laboratory controls on primary macrophages. Highly M-tropic controls (YU2, ADA) are displayed as blue bars and T-tropic controls (LAI, 4013P) are in red. Bars are representative of at least 47 independent macrophage donors. Error is displayed as mean ± SD, $^{****}P < 0.0001$ (two-tailed unpaired *t* test). Images are representative fields of each of the controls. (*D*) Fusogenicities of post-ATI–derived patient envelopes for macrophages. Fusion capacity in macrophages was assessed for ∼500 recombinant viruses from six subjects undergoing ATI (*D*, *Left*). Representative recombinants exhibiting high (greater than 50% macrophages with hydrolyzed CCF2-AM), intermediate (20 to 50%), and low (<20%) macrophage fusogenicity are indicated for each subject. Representative microscopic images for viruses designated H, I, and L are shown (*D*, *Right*). Frequencies of cells harboring hydrolyzed CCF2-AM were quantified as number of blue/total cells using ImageJ version 1.49u. Each dataset represents the mean of three independent macrophage preparations from independent donors. Graph is shown as mean ± SEM, $^{***}P < 0.0005$, $^{****}P < 0.0001$ (two-tailed Kruskal–Wallis multiple comparison). (Scale bars, 100 μm.)

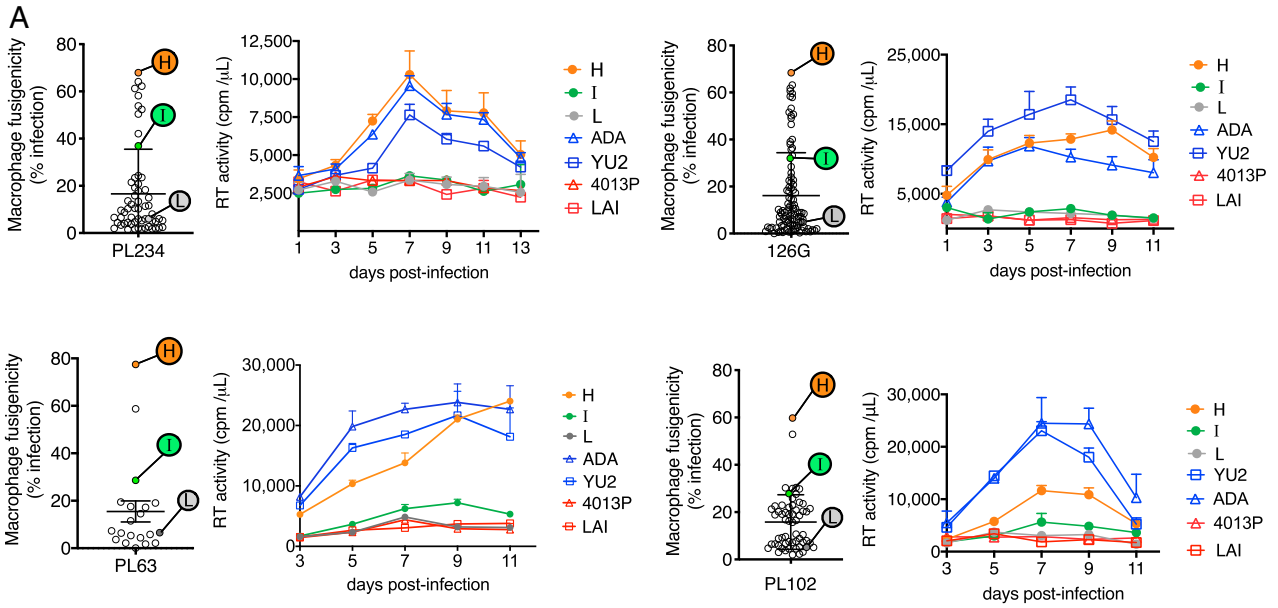

B

Summary of Phenotype

PID	# generated recombinants	# infectious in TZM-bl	# unique envelopes	# fusogenic for macrophages (> 50%)	# unique M-tropic envelopes	% M-tropic (replicating in macrophage)
PL234	71	56	29	8	3	10.3
126G	113	91	43	12	3	6.9
PL63	72	20	19	2	2	10.5
PL102	88	50	31	3	3	9.6
PL109	110	87	51	2	0	0
PL216	97	56	46	2	1	2.1

C

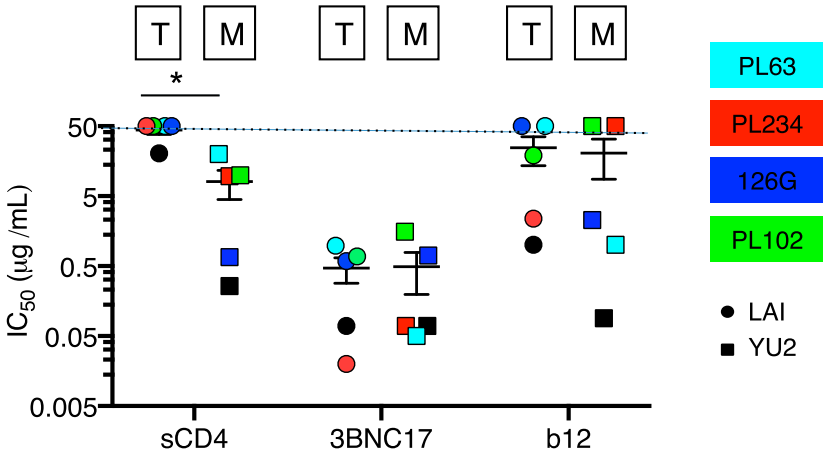

Fig. 2. Post-ATI–derived viral envelopes confer efficient replication capacity in macrophages and display increased CD4 inhibitor sensitivity. (*A*) Selected recombinant viruses with high (>50% infected macrophages), intermediate (20 to 50%), and low (<20%) capacity for fusing with macrophages were assessed for their ability to undergo spreading infection in these cells. Subject-matched Env-recombinant viruses were used to infect macrophages isolated from three independent donors. Replication was assessed by HIV-1 reverse transcriptase activity in the culture supernatants. Replication curves from subjects PL234, 126G, PL63, and PL102 are shown. Graphs are displayed as mean ± SD. (*B*) Summary of viral infectivity phenotypes assessed by fusion and replication capacity of recombinant viruses generated from six subjects undergoing ATI. (*C*) Antibody and CD4 inhibitor sensitivity of LAI, YU2, and recombinant viruses harboring PL234 (red), 126G (dark blue), PL63 (light blue), and PL102 (green) patient-derived envelopes with high (M-tropic) and low (T-tropic) macrophage fusogenicities tested in *A*. Env-recombinant viruses were exposed to increasing concentrations of soluble CD4 (sCD4), 3BNC117, and b12, in a TZM-bl neutralization assay. T- and M-tropic laboratory-adapted controls LAI and YU2 are also shown. Dashed line indicates highest antibody concentration tested. Error bars are shown as mean ± SEM, $*P < 0.05$ (two-tailed Mann–Whitney *U* test).

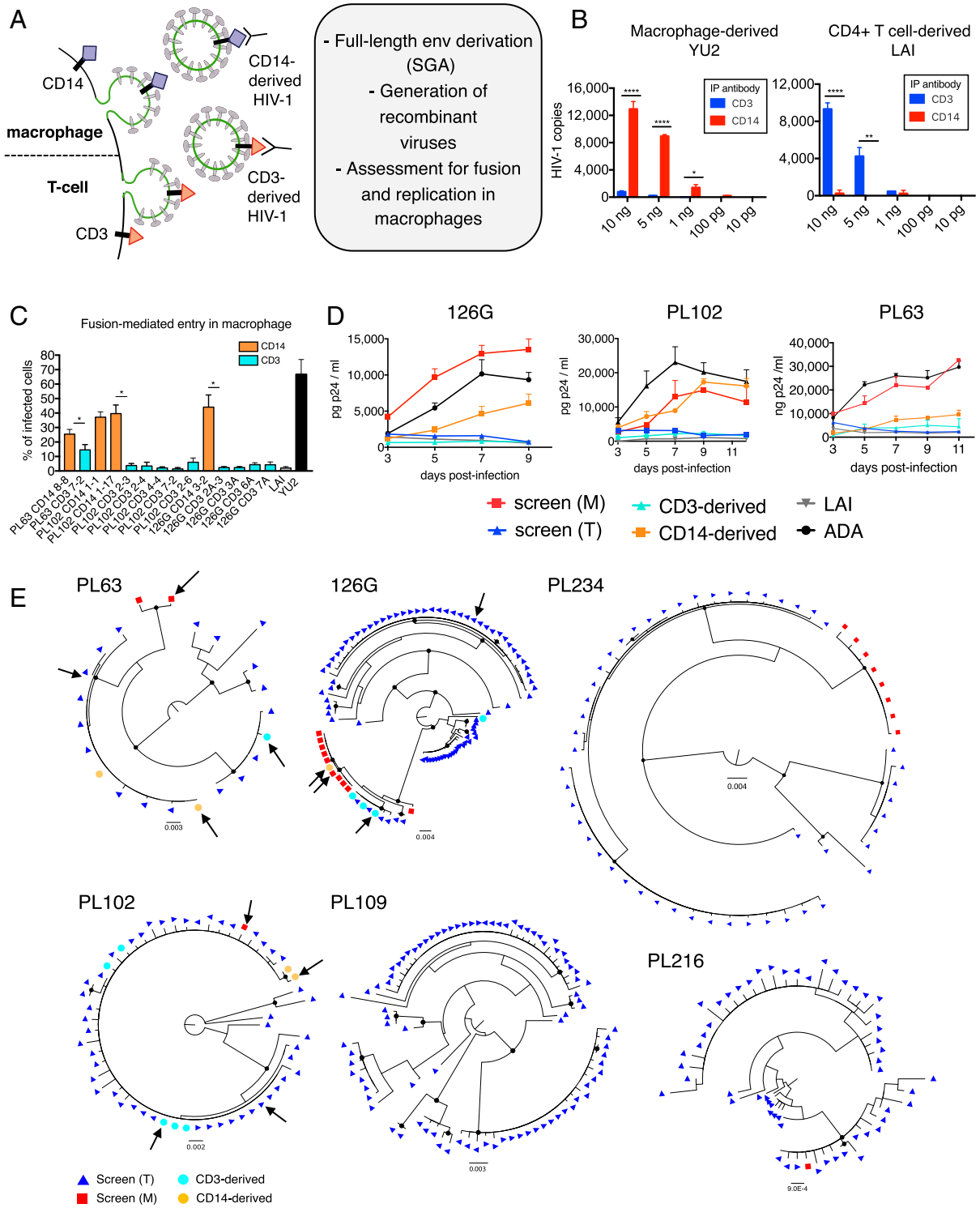

Fig. 3. HIV-1 envelopes derive from a macrophage source and consist of a genetically diverse, independent reservoir. (*A*) Rationale for antibody-mediated enrichment of macrophage-adapted virions from post-ATI plasma. Virions in post-ATI plasma were immunoprecipitated with CD14 or CD3 Ab-coupled 2.8-mm epoxy magnetic beads. (*B*) Levels of enrichment using CD3, CD14, and isotype control antibodies were assessed on virions derived in vitro from macrophages and CD4+ T cells. Total HIV-1 DNA was quantified from immunoprecipitates by RT-PCR. Error bars are representative of two independent experiments. $****P < 0.0001$, $**P < 0.01$, $*P < 0.05$ (two-way ANOVA, multiple comparison). (*C* and *D*) Viral envelopes were generated from genomic viral RNA in immunoprecipitated virions by SGA and used to construct full-length recombinant infectious viruses that were then assessed for (*C*) fusion and (*D*) replication capacity in primary macrophages. Fusion and replication capacity of recombinant viruses containing CD14- and CD3-enriched envelopes was assessed in parallel with patient-matched T- and M-tropic recombinant viruses whose envelopes had been derived by direct cloning from raw, post-ATI plasma. (*C*) Bars represent the mean of four independent replicates (mean ± SD, $*P < 0.05$; Mann–Whitney *U* test). (*D*) Error bars are representative of two (126G, PL63) or three (PL102) independent donor cells. Graphs are displayed as mean ± SEM. (*E*) Maximum-likelihood phylogenies of HIV-1 *env* sequences from all subjects sampled from post-ATI plasma. Phylogenetic trees were generated using IQ-TREE software. Arrows indicate representative infectious clones used to evaluate replication in macrophages in *D*.

envelopes derived by random screening of post-ATI plasma (Fig. 3*E*). In PL102, CD14-derived envelopes were more related to its T-tropic counterparts, suggesting recent adaptation to macrophage tropism (Fig. 3*E*). In one PL102 M-tropic envelope, one single-amino acid (AA) change (N191S) was sufficient to confer macrophage tropism in its nearest T-tropic relative (*SI Appendix*, Fig. S6). M-tropic envelopes isolated in half of our subjects (PL63, 126G, and PL234) formed distinct lineages relative to their T-tropic counterparts (Fig. 3*E*). M-tropic envelopes in PL234 and PL63 had a minimum of 12 AA that distinguish those sequences from their nearest T-tropic counterparts while in 126G, there were at least 4-AA differences between M-tropic and the nearest T-tropic counterparts (*SI Appendix*, Table S5). Even in cases where M-tropic viruses were more similar to their T-tropic counterparts, differences in the M-tropic envelopes (N191S in PL102 and N386D in 126G) have been associated with macrophage tropism (17–20). As such, minor changes in the envelope are sufficient to confer macrophage tropism and permit replication in macrophages (*SI Appendix*, Fig. S6). Thus, we conclude that M- and T-tropic viruses exhibit varying degrees of genetic differences and that M-tropic viruses detected in post-ATI plasma in three subjects (PL102, PL63, and PL126G), had a macrophage origin.

Pre-ART samples were not available for the subjects included in this study. Therefore, to assess whether M-tropic viruses identified in post-ATI viremia originated from macrophages prior to treatment interruption, we used the Bayesian phyloanatomy framework (21) enforcing a relaxed molecular clock

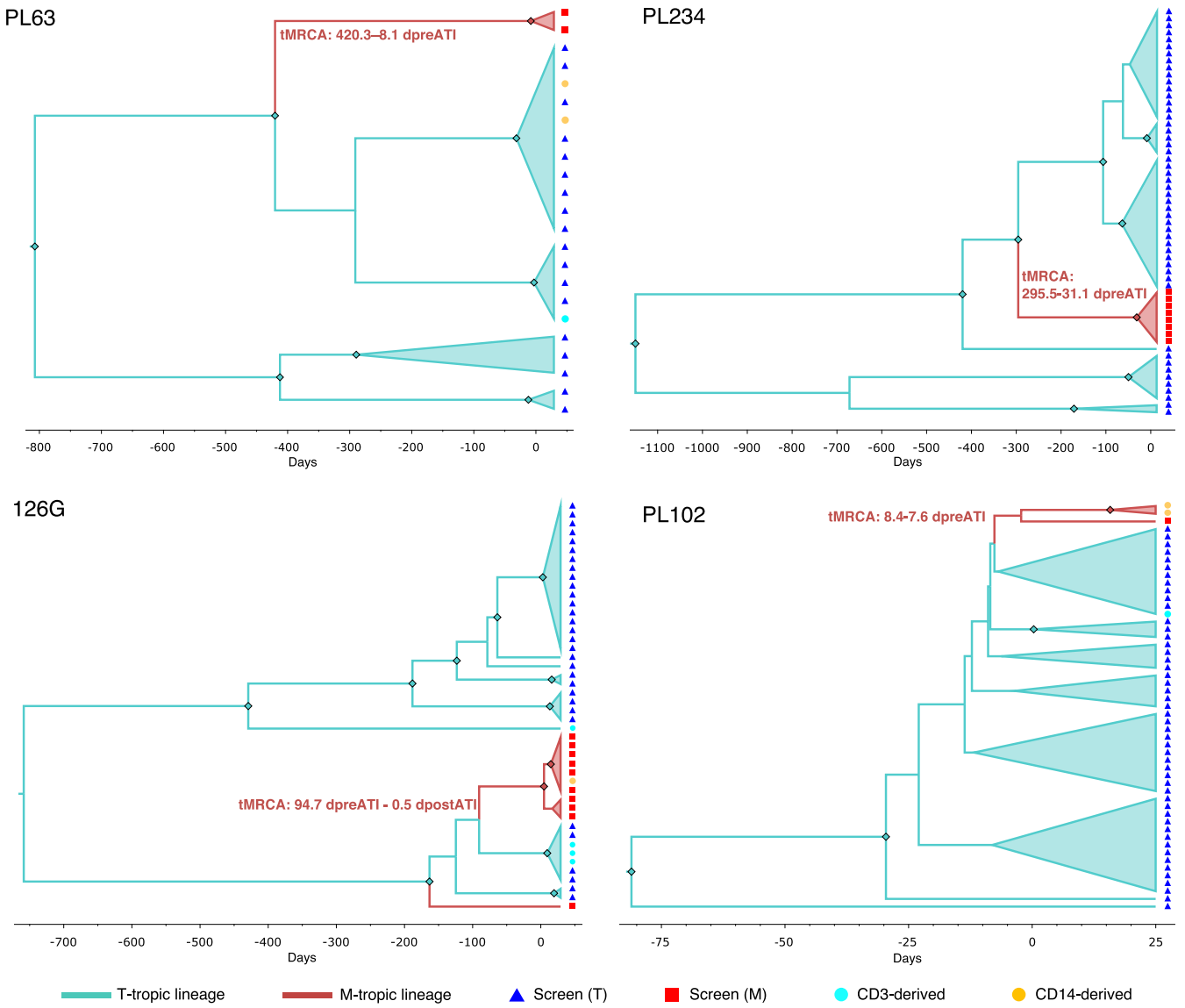

Fig. 4. Bayesian phyloanatomy analysis of HIV-1 *env* sequences from four patients sampled after therapy interruption. Maximum clade credibility trees inferred from HIV-1 *env* sequences for each patient (PL63, PL234, 126G, and PL102) were scaled in time by enforcing an uncorrelated relaxed molecular clock with prior mean evolutionary rate of $7.53{\cdot}10^{-3}$ nt substitutions per site per year (24). Timescale is in days: 0 corresponds to the time of treatment interruption, dpreATI indicates days before ART interruption, and dpostATI days post-ART interruption. Origin of the tropism at ancestors was inferred using an asymmetric phylogeographic diffusion model, implemented in BEAST v1.8.4. Branches and internal nodes are colored according to phenotype (macrophage-tropic, brown; T-tropic, cyan); the most likely phenotype of ancestral nodes/lineages was inferred using an asymmetric phylogeographic diffusion model. Diamonds represent branches supported by posterior probability >0.9, and cyan or brown colors represent probability for the ancestor of being either T-tropic or M-tropic. M-tropic sequences are indicated in red squares, T-tropic in blue triangles, and CD3- or CD14-derived are colored in light blue or yellow circles, respectively.

(22, 23), after controlling for absence of contamination and phylogenetic signal (*SI Appendix*, Figs. S8 and S9). HIV-1 time-scaled phylogenies were inferred from full-length *env* sequences of four patients (PL63, 126G, PL234, and PL102) (Fig. 4 and *SI Appendix*, Figs. S9–S11), using a robust estimate of intrahost evolutionary rate in the *env* gene ($7.53{\cdot}10^{-3}$ nt substitutions per site per year) (24). Bayesian phyloanatomy also allowed the reconstruction of the most likely ancestral phenotype (M-tropic or T-tropic) of each viral lineage in the phylogenies. We further assessed potential recombination between sequences using RDP4 software (25) and no statistically significant evidence of recombination between any of the six subjects was found. In three patients, the M-tropic lineage from which the monophyletic clades originated predated substantially therapy interruption dating back to over 1 y in PL63 (420.3 d pre-ATI), ∼10 mo in PL234 (295.5 d pre-ATI), and 3 mo in 126G (94.7 d pre-ATI) (Fig. 4 and *SI Appendix*, Table S2). In the monophyletic clade for subject 126G, the time of the most recent common ancestor (tMRCA) lies close to ATI (Fig. 4). As less than 1% of the history of the evolution of the M-tropic lineage of patient 126G occurred after treatment interruption, it is very likely that emergence of this lineage occurred before ATI. For subject PL102, the tMRCA for the M-tropic clade emerged 7.6 d before therapy interruption, with the tMRCA for the node before the divergence of the M-tropic lineage from T-tropic ones emerging 8.4 d before therapy interruption. For subject PL216, it was not possible to estimate the tMRCA, due to absence of sufficient M-tropic envelopes isolated that otherwise would provide robust power to run the molecular clock. Overall, the results indicate that M-tropic variants existed under therapy. Importantly, the relaxed molecular clock model assumes that there are no periods of latency in each lineage. Under latency, there is no opportunity for continued sequence divergence in each lineage. As such, the age of each lineage is likely an underestimate. The findings herein suggest that macrophages harbor HIV-1 in individuals on effective ART and contribute to viral rebound when ART is interrupted.

Discussion

Previous studies aimed at assessing the presence of a macrophage reservoir under suppressive ART have resorted to tissue sampling and examination for viral nucleic acids in purified macrophage populations (26–28). These studies have been hampered by limitations in tissue sampling, especially CNS tissue, in living subjects. The presence of integrated DNA in a tissue macrophage also does not prove a reservoir, since the provirus in those cells may be archival from the interval prior to treatment initiation or nonfunctional and incapable of generating biologically competent virions (29). Although it has been proposed that SIV nucleic acids detected in macrophages of infected macaques were not deposited by infection, but rather by phagocytosis of an infected CD4+ T cell (30), it has been shown that macrophages become infected following phagocytosis of infected CD4+ T cells (31). For those reasons, the issue of macrophage reservoirs has been explored primarily in animal models. Latent and productive infection of human macrophages has also been reported in a humanized mouse model, which reconstitutes tissue macrophages but not CD4+ T cells (10).

The approach taken in our study does not rely on tissue sampling and inherent limitations therein. While the plasma sampling approach is laborious, viral envelopes are derived from plasma virions. By definition therefore, the origin of those envelopes constituted a functional reservoir, i.e., one capable of producing biologically competent viruses. Although our results indicate that some of these M-tropic viruses had a direct macrophage origin, our study does not shed light on the chronicity of macrophage infection nor does it reveal the anatomic location(s) of those infected macrophages. A limitation of our study was the absence of pre-ART samples with which to gauge whether M-tropic viruses were present prior to ART. While we used a relaxed molecular clock approach to determine whether M-tropic viruses were present prior to treatment interruption, there are several caveats to the analysis that impact its interpretation. During rapid virus outgrowth, recombination and cellular proliferation that can occur following treatment interruption might give spontaneous rise to M-tropic variants. In addition, the molecular clock analysis does not accommodate the impact of latency and, as such, would provide an underestimate of the actual timing with which the M-tropic virus was established. While recombination was not detected, it is not possible to conclude whether M-tropic variants were established prior to treatment interruption particularly in subjects PL102 and PL216.

HIV-infected macrophages have been observed in multiple peripheral tissues including lung (28), lymph nodes (32), urethra (33), and liver (34). However, most of our understanding regarding the evolution of macrophage tropism has been derived from the study of viral envelope sequences obtained from the CNS of viremic individuals with late-stage disease (13, 15, 35). Those studies demonstrate that HIV-1 envelopes in the brain are highly compartmentalized from those outside the CNS and have evolved to exploit low levels of CD4 on myeloid lineage cells for infection (19, 35, 36). It is not yet known whether those compartmentalized M-tropic viruses in the CNS persist under suppressive ART. The CNS provides a privileged environment in which evolution to higher CD4 affinities would not be hindered by the presence of envelope antibodies interacting near the CD4-binding site. Furthermore, as there are few CD4+ T cells, macrophage tropism can evolve through exclusive replication in macrophages. In the periphery, where CD4+ T cells are not limiting, once macrophage tropism is acquired, there would be limited opportunity for those viruses to evolve to higher levels of CD4 affinity and macrophage tropism.

While some M-tropic envelopes diverged extensively from their nearest T cell counterparts (for example, over 12 amino acids over the gp120 region as in PL234 and PL63; *SI Appendix*, Table S5) some differed only by 1 or 2 amino acids (such as in PL102). We performed mutagenesis of the viral envelope obtained from PL102 that differs by a single amino acid from the nearest T-tropic variant isolated from the same sample and observed that mutating the T-tropic sequence (N191) to the M-tropic sequence (S191) leads to a statistically significant increase in macrophage fusogenicity. Furthermore, when M-tropic envelopes of M-tropic viruses were more similar to their T-tropic counterparts, differences in the M-tropic envelopes (N191S in PL102 and N386D in 126G) have been previously associated with macrophage tropism (17–20). This is in agreement with other studies where single-amino acid changes are sufficient to change tropism (37, 38). The fact that a T-tropic virus can acquire macrophage tropism with relatively few amino acid changes argues that extensive adaption is not absolutely required. Once a virus has acquired those amino acid changes necessary for macrophage tropism, the extent to which that M-tropic variant would further increase levels of CD4 affinity and macrophage tropism would depend on the anatomic site of the macrophage that it infected. Thus, a M-tropic virus that infects a macrophage in the CNS, where macrophages are the predominant if not exclusive target cell and where there is limited impact of neutralizing antibodies (particularly those binding near the CD4 binding site), would allow extensive macrophage-only adaptation that results in further phenotypic divergence (macrophage tropism) from their T-tropic counterparts.

Although macrophage tropism can be acquired with relatively few changes in envelope, M-tropic viruses are not frequently detected in infected individuals. M-tropic viruses can be found at low frequencies in the brain of individuals with untreated infection (39). However, in subjects with neuro-AIDS, highly

M-tropic viruses are consistently detected and form the majority of viruses detected in brain tissue (35, 36, 40, 41). Brese et al. (36) also noted that M-tropic viruses are present in brain well before neurological complications arise, which is in agreement with Sturdevant et al. (42). There is general consensus from these studies that while M-tropic viruses can rarely be found in lymphoid sites such as spleen (36), highly M-tropic viruses are more readily detectable and compartmentalized in the brain. The work of Beauparlant et al. (16) may explain the low frequency of M-tropic viruses outside the CNS. They observed that the higher CD4 affinity required for macrophage tropism comes at a fitness cost (16). Viral entry was impaired on CD4-high T cells but not on CD4-low targets, including macrophages, and had reduced shielding to neutralizing antibodies. This supports the model in which adaptation to infection of CD4-low targets such as macrophages is likely to occur in the immune-privileged site where CD4-low targets are more abundant (16). Given the negative fitness cost of M-tropic viruses in CD4+ T cells, it is possible that, during spread of the M-tropic virus beyond the original macrophage source in untreated infection, or following ATI, any recrudescing M-tropic viruses would undergo negative selection during replication in CD4+ T cells and mutations conferring macrophage tropism would be selected against. Our data demonstrate that some M-tropic viruses originate from macrophages and, in some cases, are phylogenetically distinct from their T cell tropic counterparts. However, negative pressure on M-tropic viruses during the treatment-interruption phase could account for our observation that some T-tropic viruses were similar to M-tropic viruses. In this case, the viruses have the same origin, but some progeny viruses lost their macrophage tropism during the ATI phase.

The evidence presented herein for a macrophage reservoir under ART has implications for the design of strategies with which to eliminate HIV-1 infection. Approaches adopted for the clearance of infected CD4+ T cells may be less effective in promoting the clearance of infected macrophages. As such, novel approaches may be required to clear macrophage reservoirs from HIV-1–infected individuals.

Materials and Methods

Study Subjects. The subject samples used for tropism analyses were collected during previous studies carried out at IrSiCaixa Barcelona (five patients) (43), previously approved by the Clinical Research Ethics Committee of the Hospital Germans Trias i Pujol with reference no. PI-17-042. Additionally, one subject from the ATCG A5068 study (44) was also included, under IRB approval no. 2014P000661. At the time of recruitment, patients were chronically infected with HIV-1 subtype B, on stable ART and with undetectable viral load. Written, informed consent was obtained from all subjects, following specific institutional review board-approved protocols. All experiments described in the present study were approved under IRB nos. PI-17-042 and 2014P000661. Plasma post-ATI was obtained through leukapheresis shortly after HIV-1 was detectable in the blood. Patient characteristics (age, gender, treatment, CD4 counts) are summarized in *SI Appendix*, Table S1, except for patient PL216, for which clinical information was unavailable.

Cells. TZM-bl and HEK 293T cells were maintained in Dulbecco's modified Eagle medium (DMEM) (Gibco) supplemented with 10% heat-inactivated FBS (HyClone), 2 mM L-glutamine (Gibco), 100 units/mL penicillin, and 100 μg/mL streptomycin (Sigma) at 37 °C and 5% CO_2. Monocyte-derived macrophages were isolated from elutriated blood from healthy donors. Monocytes were negatively selected using magnetic particles from the EasySep Human Monocyte CD14+ without CD16 depletion Enrichment kit (StemCell Technologies). Monocytes were differentiated in DMEM supplemented with 10% heat-inactivated human serum (Sera Care Life Sciences), 2 mM L-glutamine (Gibco), 10 μg/mL gentamicin (Sigma-Aldrich), and 12.5 ng/mL M-CSF (R&D Systems) and cultured for 7 d at 37 °C with 5% CO_2 to allow differentiation to macrophage.

Amplification of HIV-1 *env* by SGA. Viral RNA was isolated from rebound plasma of subjects undergoing ATI using the QIAamp viral RNA Mini kit (Qiagen). cDNA was generated using SuperScript III Reverse Transcriptase (Invitrogen) and HIV-1 specific primer for *env* gene 5′-TTGCTACTTGTGATTGCTCCATGT. A 2.3-kb amplicon spanning the env region was amplified by nested PCR using Taq High-Fidelity DNA polymerase (Invitrogen), first-round primers EnvB5in 5′-TTAGGCATCTCCTATGGCAGGAAGAAG and Env3Bin 5′-GTCTCGAGATACTGCTCCCACCC and second-round primers PacI/f 5′-CAGGTTAATTAATAGAATAACAGAAAGAGCAGAAGAC and BamHI/r 5′-AGATAAGTGCTAAGGATCCGTTCACTA. For site-directed mutagenesis of PL102 envelope, the following primers were used: mutM102/f 5′-GCTGATAAATTGTAGCACCTCAGTC-3′ and mutM102/r 5′-GACTGAGGTGCTACAATTTATCAGC-3′. Env gene products were purified using the QIAquick PCR purification kit (Qiagen) to further clone into an infectious HIV-1 plasmid backbone. This region was flanked by conserved PacI and BamHI sites that facilitated subsequent cloning into a modified infectious molecular clone (pLAI) as outlined below.

Generation of Infectious Molecular Clones Harboring Patient-Derived HIV-1 envelopes. HIV-1 LAI was first modified to facilitate insertion of patient-derived envelopes harboring flanking PacI and BamHI sites (Fig. 1*A*). To insert the PacI site, a 1,277-bp region of pLAI was replaced with a corresponding region derived from HIV-1 pYU2, which contains a PacI site at residue 5,766. This modified pLAI now contained 1,062 bp of pYU2 and harbored the desired PacI and BamHI sites at residues 5,766 and 8,068, respectively (Fig. 1*A*). The SGA-derived envelopes were inserted between the PacI and BamHI sites of this clone. As such, the final recombinants contained 1,062 bp of pYU2 upstream of the viral envelope start site. Within the envelope region these final SGA recombinants harbored 322 bp of pLAI (Fig. 1*A*). All envelopes, including the laboratory controls LAI, 4013P, ADA, and YU2 used in the study, were cloned into the same backbone. Therefore, all patient-derived and laboratory controls were examined in an isogenic background. This strategy faithfully preserved the phenotype of the inserted envelope. Therefore, T-tropic envelopes retained their phenotype after insertion into this isogenic background (Fig. 1*C* and *SI Appendix*, Fig. S1).

To generate virions from the env-recombinant clones, HEK 293T cells were plated at a density of 1×10^5 cells per well on a 12-well plate and incubated at 37 °C for 16 h. Cells were transfected with 1.4 μg of plasma-derived recombinant envelopes, 0.24 μg of BlaM-Vpr plasmid, and 5 μL FuGENE 6 (Promega) in opti-MEM (Sigma). After 16 h, the medium was fully changed. After 48 h, the supernatant was harvested, filtered through a 0.45-μm syringe filter (Millipore), and stored at −80 °C. Viral supernatants were titered by reverse transcriptase activity (RT assay) through incorporation of radioactive ^{3}H-dTTP.

Fusion-Mediated Entry. Env-recombinant viruses were assessed for infectivity in TZM-bl and tropism in monocyte-derived macrophages and CD4+ T cells. Briefly, TZM-bl (5×10^4 cells per well) or macrophages and CD4+ T cells (1×10^5 cells per well) were plated onto 96-well, black-walled, clear-bottomed plates. Prior to infection, cells were pretreated with 20 μg/mL of DEXTRAN for 30 min at 37 °C. Cells were infected with 5×10^5 (TZM-bl) or 1×10^6 (macrophage and CD4+ T cells) counts per minute (cpm) of the stock viral preparations for 2 h. Medium was changed and replaced with DMEM FluoroBrite (Invitrogen) in the presence of the substrate for β-lactamase, CCF2-AM, according to the manufacturer's protocol. Fusion of the virus with the cell membrane leads to release of an encapsidated Vpr-β-lactamase (βlaM-Vpr) fusion protein into the cytosol. Enzymatic cleavage of CCF2-AM by β-lactamase results in a shift in the fluorescence emission spectrum of the dye from green (520 nm) to blue (447 nm), which is then visualized by fluorescence microscopy (Fig. 1*B*). Fluorescence readout was performed 2 h after CCF2-AM was added to the cells. The number of blue/total cells was quantified using ImageJ (version 1.49u) through the establishment of a blue-green color threshold algorithm. Viral envelopes were characterized as having high (>50% positive macrophages), intermediate (20 to 50% positive macrophages), and low (<20% positive macrophages) fusogenicity.

Quantitation of uncleaved or cleaved CCF2-AM in infected macrophages or CD4+ T cells was further assessed by flow cytometry. Briefly, macrophages and CD4+ T cells were seeded onto 12-well plates at 1×10^6 cells per well or 96-well V-bottom plates at 1.5×10^6 cells per well, respectively. The next day, cells were pretreated with 20 μg/mL of DEXTRAN and infected (1×10^6 cpm virus per well). After 2 h, viruses were removed and cells were washed two times with DMEM FluoroBrite and incubated in medium with or without CCF2-AM (control wells were replaced with DMEM FluoroBrite only). Cells were washed two times with 1× PBS and stained with 1:1,000 diluted Live/Dead FarRed Fixable Dye (Invitrogen) for 30 min at room temperature. Cells were washed two times and resuspended in 4% paraformaldehyde (PHA) for 20 min. PHA was removed, and cells were washed two times, resuspended in MACS buffer (Miltenyi), and left in the dark at 4 °C overnight. The next day,

macrophages were detached from the wells with Accutase (STEMCELL Technologies) for 1 h. Cells were transferred to polypropylene tubes and washed two times with MACS buffer. CD4+ T cells were stained with anti-CD3 BV650 antibody (OKT3 clone; Biolegend) and anti-CD4 PE antibody (A161A1 clone; Biolegend) at a 1:40 dilution for 1 h at room temperature. Quantification of cleaved and uncleaved CCF2-AM was performed using BV421 and BV510 filters, respectively. All data were acquired using BD LSRII equipment (BD Biosciences) on BD FACS Diva Software (version 8.0.1).

Assessment of Viral Replication Capacity. To evaluate the ability of recombinant envelope molecular clones to replicate in macrophage, cells were plated at 2×10^5 cells per well in a 48-well plate. The next day, macrophages were infected with 1×10^6 cpm of viral stocks in the presence of 20 μg/mL of DEXTRAN. After 16 h, the medium was replaced, and an aliquot of the supernatant containing virus was harvested every other day for 12 d (50% media change at each time point). Gag p24 or reverse transcriptase levels in culture supernatants were quantitated using a commercially available p24 Enzyme Linked Immunosorbent Assay (ELISA) kit (Clontech) or by quantification of reverse transcriptase (RT) activity through incorporation of radioactive 3H-dTTP (45). Macrophage tropism was defined as envelopes with replication capacity ≥50% of that observed with M-tropic controls (YU2, ADA).

Neutralization Assay. Virus neutralization was measured using a luciferase-based assay in TZM-bl cells as previously described (46). This assay measures the reduction in luciferase reporter gene expression in TZM-bl cells following a single round of virus infection. Env-recombinant viruses were screened for neutralization sensitivity using a panel of mAb or protein reagents targeting the CD4-binding site (soluble human CD4, 3BNC117, and b12), V3-glyan (PGT121), V1/V2-glycan (PG9, PGDM1400), MPER (2F5, 4E10), or coreceptor-binding site (17b) epitopes. mAbs were tested using a primary concentration of 50 μg/mL (or 25 μg/mL for 17b) with threefold dilution series. After 48 h of infection, cells were lysed and luminescence signal was measured. The 50% inhibitory concentration (IC_{50}) titer was calculated as the mAb concentration that yielded a 50% reduction in relative luminescence units (RLU) compared to the virus control wells after subtraction of cell control RLUs.

Immunoprecipitation. HIV-1 particles present in post-ATI plasma were immunoprecipitated using 2.8-mm Epoxy magnetic beads (Invitrogen) coupled with monoclonal mouse anti-human CD3 antibody (OKT3 clone; Invitrogen) or CD14 antibody (61D3 clone; Invitrogen). Briefly, 20 μg of antibody per 1 mg of magnetic beads was coupled using an antibody-coupling kit (Invitrogen) according to the manufacturer's protocol. The bead–antibody complex was blocked with 1× PBS containing 3% bovine serum albumin (BSA) and 0.1% Tween 20 at room temperature for 1 h. To immunoprecipitate HIV-1 particles, 1.5 mg of antibody-coupled beads was mixed with 1×10^5 to 2×10^5 HIV-1 RNA copies of plasma (except for samples PL234, PL109, and PL216, for which there were not sufficient volumes of plasma) and incubated in a rotator at room temperature for 15 min. Envelopes of immunoprecipitated viruses were amplified by SGA to assess tropism in macrophages.

For validation of the assay, increasing amounts (1 pg, 10 pg, 1 ng, 5 ng, and 10 ng of p24) of macrophage-derived YU2 or CD4+ T cell-derived LAI were immunoprecipitated using 1.5 mg of either CD3 or CD14 antibody-coupled beads for 15 min in rotation at room temperature. The immunoprecipitated complex was washed four times and resuspended in 140 μL of IP buffer. Immunoprecipitates were lysed and RNA extracted using the QIAamp viral RNA Mini kit. cDNA was generated using SuperScript III reverse transcriptase and random hexamer primers. To quantify total HIV-1 DNA, 2 μL of cDNA was incubated with forward primer C1r 5′-TCC CAG GCT CAG ATC TGG TCT A-3′, reverse primer C4r 5′-CTT CCC TGA TTG GCA GAA CTA C-3′, and 2n4n probe 5′-/56-FAM/AG TGG CGA G/ZEN/C CCT CAG ATG CTG C/3IABkFQ/-3′, in the presence of TaqMan Fast Universal Master Mix (Applied Biosystems). Detection of total HIV-1 DNA was performed using a QuantStudio 6 Flex Real-Time PCR System.

***Env* Sequencing and Phylogenetic Trees.** A 2.3-kb region of HIV-1 *env* was sequenced from purified plasmid DNA. The primers used for env amplification include PacFN/f 5′-CAGGTTAATTAATAGAATAACAGAAAGAGCAGAAGAC, BamRS/r 5′-AGATAAGTGCTAAGGATCCGTTCACTA, LA9/f 5′-ACATGCCTGTGTACCCACAGA, LA12/f 5′-ATGGCAGTCTAGCAGAAGAAGA, Env2/r 5′-CCTCCAGGTCTGAAGATCTC, Env5/f 5′-GGCGCAACAGCATCTGTTGCA, Env6/r 5′-TGCGTCCCAGAAGTTCCACAA, and Env4/f 5′-ACAATCACACTCCCATGCAGA. Sequenced envelopes were assembled using Sequencher v5.4.6 and aligned using the MUSCLE algorithm (47, 48) implemented in MEGA7 (49) and manually edited to codon-based nucleotide alignments.

Phylogenetic relationships among the *env* sequences were reconstructed by inferring a maximum-likelihood (ML) tree, using the best-fitting evolutionary model chosen according to Bayesian information criteria (BIC), with the IQ-TREE software (50). The tree showed sequences from each patient clustering in separate, and highly supported, monophyletic clades (*SI Appendix*, Fig. S7). Presence of nucleotide substitution saturation, which decreases the phylogenetic information contained in the sequences, was assessed by plotting pairwise transition and transversion substitutions versus genetic distance with the program DAMBE6 (51) (*SI Appendix*, Fig. S8*A*). Likelihood mapping analysis implemented in IQ-TREE (50, 52) was also used to evaluate the presence of sufficient phylogenetic signal to resolve evolutionary relationships among the sequences (*SI Appendix*, Fig. S8*B*). Intraclade and inter–M- or –T-tropic group average genetic distances, as well as pairwise genetic distance across all sequences (*SI Appendix*, Table S3), were calculated using ML-composite estimated distances with SE obtained by bootstrapping (1,000 replicates) in MEGA7 (49). For each patient-specific dataset, a posterior distribution of HIV-1 phylogenies was inferred with the Bayesian framework implemented in BEAST v1.8.4 (53), by enforcing the HKY or general time-reversible (GTR) nucleotide substitution model, an uncorrelated molecular relaxed clock, assuming a mean HIV-1 intrahost evolutionary rate of $7.53 \cdot 10^{-3}$ nt substitutions per site per year (24) and a Bayesian skyline plot or constant as demographic priors. Marginal-likelihood estimates (MLE) were obtained using path sampling (PS) and stepping-stone sampling (SS) methods to test whether the HKY or the GTR model was the best nucleotide substitution model to use. The strength of evidence against the null hypothesis (H_0) was evaluated via MLE comparison with the more complex model (H_A), referred to as the Bayes factor (BF), wherein $ln\text{BF} < 2$ indicates no evidence against H_0; 2 to 6, weak evidence; 6 to 10, strong evidence; and >10, very strong evidence (54, 55). The HKY nucleotide substitution model was the best compared to the GTR nucleotide substitution model (*SI Appendix*, Table S4). Viral phenotypes (M- or T-tropic) were treated as discrete traits to allow the reconstruction of ancestral phenotypes along the trees by using the asymmetric transition model implemented in BEAST (56). For each dataset, a Markov chain Monte Carlo was run for 200, 400, or 800 million generations, sampling every 20,000, 40,000, or 80,000 generations. Proper mixing of the Markov chain was assessed by calculating the effective sampling size of each parameter estimate, which resulted in >200 for all parameters at the end of the run, after 10% burn-in. Finally, a maximum clade credibility (MCC) tree was calculated, for each dataset, from the posterior distribution with TreeAnnotator in the BEAST package. Phylogenetic trees were analyzed and graphically edited in FigTree v1.4.2 (http://tree.bio.ed.ac.uk/software/figtree/). Xml files are available upon request.

Identification of putative recombinant sequences was performed using the RDP, GENECONV, BootScan, MaxChi, CHIMAERA, SIScan, and 3Seq algorithms implemented in the RDP4 software (25) (http://web.cbio.uct.ac.za/~darren/rdp.html). Recombination events were considered as such if supported by at least six of the seven algorithms used. No evidence of recombination among the sequences obtained from the six patients was found. Statistical evidence of recombination was indicated by P values <0.05, and default settings were used with linear genome specification.

Statistical Analysis. All data were analyzed using GraphPad prism 7, excluding sequencing phylogeny data. P values of 0.05 or less were considered statistically significant. A two-tailed, unpaired Student's t test was applied to evaluate statistical significance in Fig. 1*C*. A nonparametric, two-tailed Mann–Whitney U or Kruskal–Wallis (for multiple comparisons) test was applied to evaluate statistical significance in Figs. 1*D*, 2*C*, and 3*C* and *SI Appendix*, Figs. S1 and S4*A*. Two-way ANOVA (multiple comparisons) was used to evaluate statistical significance in Fig. 3*B*.

Data Availability. All sequences reported in this paper have been deposited in the GenBank database, under the following accession numbers: 126G (MK250122–MK250216), PL102 (MK250217–250273), PL109 (MK250274–MK250362), PL216 (MK254784–MK254839), PL63 (MN395385 and MK250100–MK250121), and PL234 (MK254843, MK254890–MK254895, MK254897, MK254911, MK254912, MK254914–MK254952, MK254959–MK254964, and MK254967).

ACKNOWLEDGMENTS. We are grateful to all subjects who contributed to the study and to the site staff involved in ACTG A5068. We thank D. Watkins, F. Cunyat, T. Plitnik, J. Salinas, R. Desrosiers, and M. McCune for advice and helpful discussions. This work was supported by grants from the NIH, including grants from the National Institute of Mental Health (P01 MH10094 and MH116701) as well as the National Institute of Allergy and Infectious

Diseases (AI12065631, P01 M1700364, PO1-AI131568, and grants funded to ACTG (AIDS Clinical Trials Group): UM1 AI068634, UM1 AI068636, and UM1 AI106701; to J.Z.L.) and the National Institute of Neurological Disease and Stroke (NS063897). Assay and reagent support was provided by the Miami Center for AIDS Research at the University of Miami Miller School of Medicine, which is funded by Grant P30AI073961 from the NIH.

1. D. Finzi *et al*., Identification of a reservoir for HIV-1 in patients on highly active antiretroviral therapy. *Science* **278**, 1295–1300 (1997).
2. T. W. Chun *et al*., Early establishment of a pool of latently infected, resting CD4(+) T cells during primary HIV-1 infection. *Proc. Natl. Acad. Sci. U.S.A.* **95**, 8869–8873 (1998).
3. D. D. Ho, T. R. Rota, M. S. Hirsch, Infection of monocyte/macrophages by human T lymphotropic virus type III. *J. Clin. Invest.* **77**, 1712–1715 (1986).
4. S. Koenig *et al*., Detection of AIDS virus in macrophages in brain tissue from AIDS patients with encephalopathy. *Science* **233**, 1089–1093 (1986).
5. T. Igarashi *et al*., Macrophage are the principal reservoir and sustain high virus loads in rhesus macaques after the depletion of CD4+ T cells by a highly pathogenic simian immunodeficiency virus/HIV type 1 chimera (SHIV): Implications for HIV-1 infections of humans. *Proc. Natl. Acad. Sci. U.S.A.* **98**, 658–663 (2001).
6. Y. Li *et al*., SIV infection of lung macrophages. *PLoS One* **10**, e0125500 (2015).
7. C. R. Avalos *et al*., Brain macrophages in simian immunodeficiency virus-infected, antiretroviral-suppressed macaques: A functional latent reservoir. *MBio* **8**, e01186-17 (2017).
8. S. V. Westmoreland *et al*., SIV vpx is essential for macrophage infection but not for development of AIDS. *PLoS One* **9**, e84463 (2014).
9. L. Micci *et al*., CD4 depletion in SIV-infected macaques results in macrophage and microglia infection with rapid turnover of infected cells. *PLoS Pathog.* **10**, e1004467 (2014).
10. J. B. Honeycutt *et al*., HIV persistence in tissue macrophages of humanized myeloid-only mice during antiretroviral therapy. *Nat. Med.* **23**, 638–643 (2017).
11. L. K. Vibholm *et al*., Characterization of intact proviruses in blood and lymph node from HIV-infected individuals undergoing analytical treatment interruption. *J. Virol.* **93**, e01920-18 (2019).
12. F. Kazazi, J. M. Mathijs, P. Foley, A. L. Cunningham, Variations in CD4 expression by human monocytes and macrophages and their relationships to infection with the human immunodeficiency virus. *J. Gen. Virol.* **70**, 2661–2672 (1989).
13. S. B. Joseph *et al*., Quantification of entry phenotypes of macrophage-tropic HIV-1 across a wide range of CD4 densities. *J. Virol.* **88**, 1858–1869 (2014).
14. M. Cavrois, C. De Noronha, W. C. Greene, A sensitive and specific enzyme-based assay detecting HIV-1 virion fusion in primary T lymphocytes. *Nat. Biotechnol.* **20**, 1151–1154 (2002).
15. G. Schnell, S. Spudich, P. Harrington, R. W. Price, R. Swanstrom, Compartmentalized human immunodeficiency virus type 1 originates from long-lived cells in some subjects with HIV-1-associated dementia. *PLoS Pathog.* **5**, e1000395 (2009).
16. D. Beauparlant *et al*., Delineating CD4 dependency of HIV-1: Adaptation to infect low level CD4 expressing target cells widens cellular tropism but severely impacts on envelope functionality. *PLoS Pathog.* **13**, e1006255 (2017).
17. A. G. Holman, M. E. Mefford, N. O'Connor, D. Gabuzda, HIVBrainSeqDB: A database of annotated HIV envelope sequences from brain and other anatomical sites. *AIDS Res. Ther.* **7**, 43 (2010).
18. M. E. Mefford, K. Kunstman, S. M. Wolinsky, D. Gabuzda, Bioinformatic analysis of neurotropic HIV envelope sequences identifies polymorphisms in the gp120 bridging sheet that increase macrophage-tropism through enhanced interactions with CCR5. *Virology* **481**, 210–222 (2015).
19. R. L. Dunfee, E. R. Thomas, D. Gabuzda, Enhanced macrophage tropism of HIV in brain and lymphoid tissues is associated with sensitivity to the broadly neutralizing CD4 binding site antibody b12. *Retrovirology* **6**, 69 (2009).
20. R. L. Dunfee *et al*., Loss of the N-linked glycosylation site at position 386 in the HIV envelope V4 region enhances macrophage tropism and is associated with dementia. *Virology* **367**, 222–234 (2007).
21. M. Salemi, B. Rife, Phylogenetics and phyloanatomy of HIV/SIV intra-host compartments and reservoirs: The key role of the central nervous system. *Curr. HIV Res.* **14**, 110–120 (2016).
22. A. J. Drummond, S. Y. Ho, M. J. Phillips, A. Rambaut, Relaxed phylogenetics and dating with confidence. *PLoS Biol.* **4**, e88 (2006).
23. R. W. Gruessner, D. E. Sutherland, A. C. Gruessner, Mortality assessment for pancreas transplants. *Am. J. Transplant.* **4**, 2018–2026 (2004).
24. P. Lemey, A. Rambaut, O. G. Pybus, HIV evolutionary dynamics within and among hosts. *AIDS Rev.* **8**, 125–140 (2006).
25. D. P. Martin, B. Murrell, M. Golden, A. Khoosal, B. Muhire, RDP4: Detection and analysis of recombination patterns in virus genomes. *Virus Evol.* **1**, vev003 (2015).
26. S. K. Cribbs, J. Lennox, A. M. Caliendo, L. A. Brown, D. M. Guidot, Healthy HIV-1-infected individuals on highly active antiretroviral therapy harbor HIV-1 in their alveolar macrophages. *AIDS Res. Hum. Retroviruses* **31**, 64–70 (2015).
27. A. Zalar *et al*., Macrophage HIV-1 infection in duodenal tissue of patients on long term HAART. *Antiviral Res.* **87**, 269–271 (2010).
28. K. C. Jambo *et al*., Small alveolar macrophages are infected preferentially by HIV and exhibit impaired phagocytic function. *Mucosal Immunol.* **7**, 1116–1126 (2014).
29. Y. C. Ho *et al*., Replication-competent noninduced proviruses in the latent reservoir increase barrier to HIV-1 cure. *Cell* **155**, 540–551 (2013).
30. N. Calantone *et al*., Tissue myeloid cells in SIV-infected primates acquire viral DNA through phagocytosis of infected T cells. *Immunity* **41**, 493–502 (2014).
31. A. E. Baxter *et al*., Macrophage infection via selective capture of HIV-1-infected CD4+ T cells. *Cell Host Microbe* **16**, 711–721 (2014).
32. S. A. Yukl *et al*., The distribution of HIV DNA and RNA in cell subsets differs in gut and blood of HIV-positive patients on ART: Implications for viral persistence. *J. Infect. Dis.* **208**, 1212–1220 (2013).
33. Y. Ganor *et al*., HIV-1 reservoirs in urethral macrophages of patients under suppressive antiretroviral therapy. *Nat. Microbiol.* **4**, 633–644 (2019).
34. A. Mosoian *et al*., Frontline science: HIV infection of kupffer cells results in an amplified proinflammatory response to LPS. *J. Leukoc. Biol.* **101**, 1083–1090 (2017).
35. M. P. Gonzalez-Perez *et al*., Independent evolution of macrophage-tropism and increased charge between HIV-1 R5 envelopes present in brain and immune tissue. *Retrovirology* **9**, 20 (2012).
36. R. L. Brese *et al*., Ultradeep single-molecule real-time sequencing of HIV envelope reveals complete compartmentalization of highly macrophage-tropic R5 proviral variants in brain and CXCR4-using variants in immune and peripheral tissues. *J. Neurovirol.* **24**, 439–453 (2018).
37. R. L. Dunfee *et al*., The HIV Env variant N283 enhances macrophage tropism and is associated with brain infection and dementia. *Proc. Natl. Acad. Sci. U.S.A.* **103**, 15160–15165 (2006).
38. T. Musich *et al*., A conserved determinant in the V1 loop of HIV-1 modulates the V3 loop to prime low CD4 use and macrophage infection. *J. Virol.* **85**, 2397–2405 (2011).
39. M. P. Gonzalez-Perez *et al*., Identification of emerging macrophage-tropic HIV-1 R5 variants in brain tissue of AIDS patients without severe neurological complications. *J. Virol.* **91**, e00755-17 (2017).
40. P. J. Peters *et al*., Biological analysis of human immunodeficiency virus type 1 R5 envelopes amplified from brain and lymph node tissues of AIDS patients with neuropathology reveals two distinct tropism phenotypes and identifies envelopes in the brain that confer an enhanced tropism and fusigenicity for macrophages. *J. Virol.* **78**, 6915–6926 (2004).
41. P. J. Peters *et al*., Non-macrophage-tropic human immunodeficiency virus type 1 R5 envelopes predominate in blood, lymph nodes, and semen: Implications for transmission and pathogenesis. *J. Virol.* **80**, 6324–6332 (2006).
42. C. B. Sturdevant *et al*., Compartmentalized replication of R5 T cell-tropic HIV-1 in the central nervous system early in the course of infection. *PLoS Pathog.* **11**, e1004720 (2015).
43. L. Ruiz *et al*.; TIBET Study Group, Antiretroviral therapy interruption guided by CD4 cell counts and plasma HIV-1 RNA levels in chronically HIV-1-infected patients. *AIDS* **21**, 169–178 (2007).
44. J. M. Jacobson *et al*.; National Institute of Allergy and Infectious Diseases-AIDS Clinical Trials Group 5068 Protocol Team, Evidence that intermittent structured treatment interruption, but not immunization with ALVAC-HIV vCP1452, promotes host control of HIV replication: The results of AIDS clinical trials group 5068. *J. Infect. Dis.* **194**, 623–632 (2006).
45. T. J. Dueweke *et al*., A mutation in reverse transcriptase of bis(heteroaryl)piperazine-resistant human immunodeficiency virus type 1 that confers increased sensitivity to other nonnucleoside inhibitors. *Proc. Natl. Acad. Sci. U.S.A.* **90**, 4713–4717 (1993).
46. M. Sarzotti-Kelsoe *et al*., Optimization and validation of the TZM-bl assay for standardized assessments of neutralizing antibodies against HIV-1. *J. Immunol. Methods* **409**, 131–146 (2014).
47. R. C. Edgar, MUSCLE: Multiple sequence alignment with high accuracy and high throughput. *Nucleic Acids Res.* **32**, 1792–1797 (2004).
48. R. C. Edgar, MUSCLE: A multiple sequence alignment method with reduced time and space complexity. *BMC Bioinformatics* **5**, 113 (2004).
49. S. Kumar, G. Stecher, K. Tamura, MEGA7: Molecular evolutionary genetics analysis version 7.0 for bigger datasets. *Mol. Biol. Evol.* **33**, 1870–1874 (2016).
50. L. T. Nguyen, H. A. Schmidt, A. von Haeseler, B. Q. Minh, IQ-TREE: A fast and effective stochastic algorithm for estimating maximum-likelihood phylogenies. *Mol. Biol. Evol.* **32**, 268–274 (2015).
51. X. Xia, Z. Xie, DAMBE: Software package for data analysis in molecular biology and evolution. *J. Hered.* **92**, 371–373 (2001).
52. J. Trifinopoulos, L. T. Nguyen, A. von Haeseler, B. Q. Minh, W-IQ-TREE: A fast online phylogenetic tool for maximum likelihood analysis. *Nucleic Acids Res.* **44**, W232–W235 (2016).
53. A. J. Drummond, A. Rambaut, BEAST: Bayesian evolutionary analysis by sampling trees. *BMC Evol. Biol.* **7**, 214 (2007).
54. G. Baele *et al*., Improving the accuracy of demographic and molecular clock model comparison while accommodating phylogenetic uncertainty. *Mol. Biol. Evol.* **29**, 2157–2167 (2012).
55. W. Xie, P. O. Lewis, Y. Fan, L. Kuo, M. H. Chen, Improving marginal likelihood estimation for Bayesian phylogenetic model selection. *Syst. Biol.* **60**, 150–160 (2011).
56. K. Strimmer, O. G. Pybus, Exploring the demographic history of DNA sequences using the generalized skyline plot. *Mol. Biol. Evol.* **18**, 2298–2305 (2001).